Synthesis of Voltage-Sensitive Optical Signals: Application to Panoramic Optical Mapping

Martin J. Bishop,* Blanca Rodriguez,* James Eason,† Jonathan P. Whiteley,* Natalia Trayanova,‡ and David J. Gavaghan*

*Oxford University Computing Laboratory, Oxford, United Kingdom; †Washington and Lee University, Lexington, Virginia; and ‡Tulane University, New Orleans, Louisiana

ABSTRACT Fluorescent photon scattering is known to distort optical recordings of cardiac transmembrane potentials; however, this process is not well quantified, hampering interpretation of experimental data. This study presents a novel model, which accurately synthesizes fluorescent recordings over the irregular geometry of the rabbit ventricles. Using the model, the study aims to provide quantification of fluorescent signal distortion for different optical characteristics of the preparation and of the surrounding medium. A bi-domain representation of electrical activity is combined with finite element solutions to the photon diffusion equation simulating both the excitation and emission processes, along with physically realistic boundary conditions at the epicardium, which allow simulation of different experimental setups. We demonstrate that distortion in the optical signal as a result of fluorescent photon scattering is truly a three-dimensional phenomenon and depends critically upon the geometry of the preparation, the scattering properties of the tissue, the direction of wavefront propagation, and the specifics of the experimental setup. Importantly, we show that in an anatomically accurate model of ventricular geometry and fiber orientation, the morphology of the optical signal does not provide reliable information regarding the intramural direction of wavefront propagation. These findings underscore the potential of the new model in interpreting experimental data.

INTRODUCTION

Over the last decade, the optical mapping technique has revolutionized research in cardiac electrophysiology due to its unique ability to provide simultaneous, noninvasive recordings of transmembrane potential from multiple sites over the surface of the heart. The technique uses voltage-sensitive fluorescent dyes that bind to the membranes of excitable cells (1). Upon illumination at the correct wavelength, these dye molecules become excited and fluoresce, transducing changes in the transmembrane potential as changes in fluorescent emission. The emitted photon flux exiting the tissue surface is recorded by an array of detectors close to the epicardium (2). However, as the illuminating light penetrates into the myocardium (up to a few millimeters (3)), the detected signal contains fluorescent photons originating not only from several millimeters directly beneath the recording site (3), but also from a widely distributed three-dimensional volume surrounding it, with the photons encountering multiple scattering events in the tissue before exiting the surface (4).

The magnitude of the fluorescent signal distortion due to photon scattering depends on a variety of factors including the characteristics of the optical mapping setup and the properties of the tissue sample, as well as the direction of wavefront propagation with respect to the recording surface. Understanding the role of these factors in modulating the fluorescent signal is essential for experimental data interpretation. Recent mathematical modeling studies have demonstrated that photon scattering in the tissue depth results in prolongation of the optical action potential upstroke and in an increase in the width of the optically recorded excitation wavefront (5,6). In addition, studies by Hyatt et al. (5,7) showed that subsurface wavefront orientation alters the duration and morphology of the optical action potential upstroke. However, these studies sought analytical solutions, and thus used geometrically simplistic domains with unrealistic boundary conditions, thereby limiting the applicability of the approach to analysis of actual optical mapping experiments.

The goals of this study are 1), to simulate the fluorescent signals recorded over the entire epicardium of the rabbit ventricles in a panoramic optical mapping experiment; and 2), to provide quantification of fluorescent signal distortion for different optical characteristics of the medium surrounding the heart and of the tissue sample itself. To do so, we use a novel anatomically based finite-element rabbit ventricular model, which combines a bi-domain model of electrical activity with a photon transport model of illumination and fluorescence. The model includes realistic representation of the optical properties of the interface between the heart and the surrounding medium through the implementation of a partial current boundary condition that can be adapted to represent different types of experimental setups.

METHODS

Computational model

The anatomically based finite-element model of the rabbit ventricles described in a previous study (8) was used to solve the equations governing

Submitted October 24, 2005, and accepted for publication December 14, 2005.

Address reprint requests to D. J. Gavaghan, Tel.: 44-1865-281-899; Fax: 44-1865-273-839; E-mail: david.gavaghan@comlab.ox.ac.uk.

0006-3495/06/04/2938/08 $2.00

doi: 10.1529/biophysj.105.076505

both electrical activation and photon scattering during the processes of illumination and emission. The myocardial mesh incorporated realistic geometry and fiber orientation, and also included representation of the perfusing bath and the blood in the ventricular cavities.

Electrical activation model

The distribution of transmembrane potential (V_m) throughout the ventricles was calculated using the bi-domain equations

$$\nabla \cdot (\hat{\sigma}_i \nabla V_m) + \nabla \cdot [(\hat{\sigma}_i + \hat{\sigma}_e)\phi_e] = -I_0, \quad (1)$$

$$\nabla \cdot (\hat{\sigma}_e \nabla \phi_e) = -I_m - I_0, \quad (2)$$

$$V_m = \phi_i - \phi_e, \quad (3)$$

where ϕ_i and ϕ_e are the intracellular and extracellular potentials, respectively; $\hat{\sigma}_i$ and $\hat{\sigma}_e$ are intracellular and extracellular conductivity tensors; and I_m and I_0 are the volume densities of the transmembrane and stimulus currents, respectively. Membrane kinetics was represented by a modification of the Luo-Rudy dynamic model (9). A stimulus of twice threshold and 4-ms duration was applied at a basic cycle length of 250 ms. Two types of stimulation resulting in different directions of wavefront propagation with respect to the epicardium were considered: 1), epicardial pacing with a 2-cm^2 electrode located at the apex; and 2), stimulation over the entire endocardium roughly approximating normal activation through the Purkinje network.

Fluorescent scattering model

We calculated both the photon density due to uniform excitation illumination (Φ_{illum}) and the photon density due to voltage-sensitive fluorescent emission (Φ_{em}) at all points within the three-dimensional volume of the ventricles using the steady-state photon diffusion equation for highly scattering media (10),

$$D\nabla^2\Phi(\mathbf{r}) - \mu_a\Phi(\mathbf{r}) = -w(\mathbf{r}), \quad (4)$$

where Φ is the photon density at any point in the tissue with position vector $\mathbf{r}$ (mm), D (mm), and μ_a (mm^{-1}) are the optical diffusivity and absorptivity, respectively, and w describes the photon source at position $\mathbf{r}$.

The effect of uniform illumination of the epicardium was calculated by solving Eq. 4 with zero source term w within the myocardium and constant epicardial boundary condition of $\Phi_{illum} = \Phi_0$, where Φ_0 is the uniformly applied illumination. The optical parameter values of the rabbit myocardium were taken at the illumination wavelength, 488 nm, of the dye di-4-ANEPPS (the most commonly used fluorescent dye in optical mapping experiments); these were $D^{illum} = 0.18$ mm and $\mu_a^{illum} = 0.52\text{mm}^{-1}$ (4).

Voltage-dependent fluorescent emission, resulting from excitation by the illuminating light, was calculated at each time step of the V_m calculation using Eq. 4 with $w = V_m\Phi_{illum}$ and values of the optical parameters taken at 669 nm, the di-4-ANEPPS emission wavelength, $D^{em} = 0.34$ mm, and $\mu_a^{em} = 0.10\text{mm}^{-1}$ for rabbit myocardium (4). For both illumination and emission, we assumed that the optical properties of the blood are equal to those of the myocardium (11).

A partial current boundary condition applied at the epicardial surface was used in the calculation of Φ_{em}

$$\Phi_{em} = 2D^{em}\frac{1 + R_{eff}}{1 - R_{eff}}\nabla\Phi_{em} \cdot \mathrm{n}, \quad (5)$$

where R_{eff} is the effective reflection coefficient, which depends on the relative refractive indices of the tissue and the surrounding medium (10); $\mathbf{n}$ is the unit vector normal to the epicardial surface. Unless otherwise stated, we assumed air surrounding the heart. Taking the refractive indices for air and cardiac tissue as $n_{air} = 1$ and $n_{tissue} = 1.4$, the formulation for R_{eff} in Haskell et al. (10) yields a control value of $R_{eff} = 0.49$. The partial current boundary condition was chosen as a more physically realistic alternative to the previously used zero boundary condition which simply imposed the constraint of $\Phi_{em} = 0$ on the epicardial surface (5,7,12).

The recorded optical signal (V_{opt}) was calculated at every epicardial node at each time step from the flux exiting the epicardial surface by applying Fick's law (5),

$$V_{opt} = -D^{em}\nabla\Phi_{em} \cdot \mathbf{n}. \quad (6)$$

Uniform, ideal detection was assumed, which approximates the conditions in panoramic optical mapping experimental setups (13–16).

Data analysis

V_{opt} signals were normalized at each node using the maximum and minimum action potential values for that node, as in experimental recordings (16). We defined the upstroke duration of the action potential as the time interval between 10 and 90% of depolarization, and we calculated τ_{opt} as the ratio of the V_{opt} to the V_m upstroke duration. During depolarization the epicardial activation wavefront width was defined as the mean percentage of surface nodes (closely related to the percentage of epicardial surface area) being on the upstroke of the action potential. We denoted the ratio of the V_{opt} wavefront width to the V_m wavefront width by ω_{opt}. Average values of τ_{opt} and ω_{opt} were calculated over the epicardial surface. Note that nodes where epicardial breakthrough occurred within the first six milliseconds were excluded due to inaccuracies in the calculation of the optical action potential upstroke duration, as a result of stimulation artifacts. These artifacts arise during the endocardial stimulation protocol in areas where the myocardial wall is so thin that the entire volume of myocardium is rapidly excited within a few milliseconds of the stimulus. As the optical action potential upstroke can be prolonged by several milliseconds, the optical action potential foot is poorly defined in these areas, meaning that accurate measurement of upstroke duration for these areas is impossible.

RESULTS

Fig. 1 *A* shows the distribution of the photon density Φ_{illum} in the three-dimensional volume of the ventricles after uniform epicardial illumination. In Fig. 1 *B*, Φ_{illum} at each node is plotted against the minimum distance from that node to the epicardium (r_{min}). Both panels in Fig. 1 show that light attenuation in cardiac tissue leads to a decrease in Φ_{illum} with increasing depth into the myocardial wall. Attenuation can be approximated by a monoexponential decay function $\Phi_{illum} = \Phi_0 e^{-r_{min}/\delta}$ with penetration depth $\delta = 0.57$ mm, also plotted in Fig. 1 *B*. Once excited by the illuminating photons, the dye molecules give out fluorescence in direct proportion to the changes in the local transmembrane potential V_m. Fig. 2 presents V_m activation maps for each of the stimulation protocols: apical stimulation elicits wavefront propagation from apex to base (*left*), while, after endocardial stimulation, propagation ensues in the direction from endo- to epicardium (*right*), traversing first the thinner RV wall.

The distribution of Φ_{illum} shown in Fig. 1 and the V_m distribution obtained from the bi-domain simulations were used to calculate the epicardial V_{opt} distribution for each stimulation protocol. Fig. 3 *A* shows the time course of V_m and V_{opt} at the node marked *X* in Fig. 2 for apical (*top*) and endocardial (*bottom*) stimulation. The main difference between the V_m and the V_{opt} traces occurs during the upstroke,

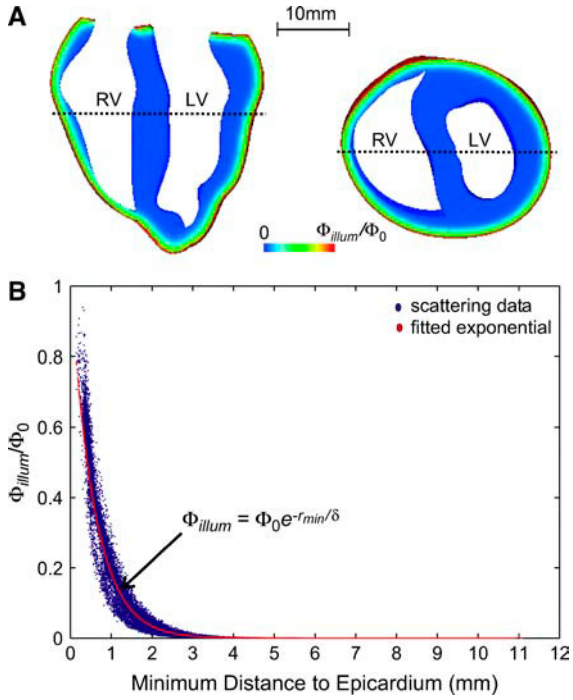

FIGURE 1 (*A*) Distribution of Φ_{illum} throughout the three-dimensional volume of the ventricles due to uniform epicardial illumination, showing the attenuation of the signal with depth into the myocardial wall. Locations of the slices through the ventricles are shown to be: apex-base (*left*) and anterior-posterior (*right*). The dashed-line in the apex-base slice refers to the position of the anterior-posterior slice; the dashed-line in the anterior-posterior slice refers to the position of the apex-base slice. (*B*) Plot of Φ_{illum} at each node point against the minimum geometric distance (r_{min}) of that point from the epicardium, along with a monoexponential decay function $\Phi_{illum} = \Phi_0 e^{-r_{min}/\delta}$ with $\delta = 0.57$ mm.

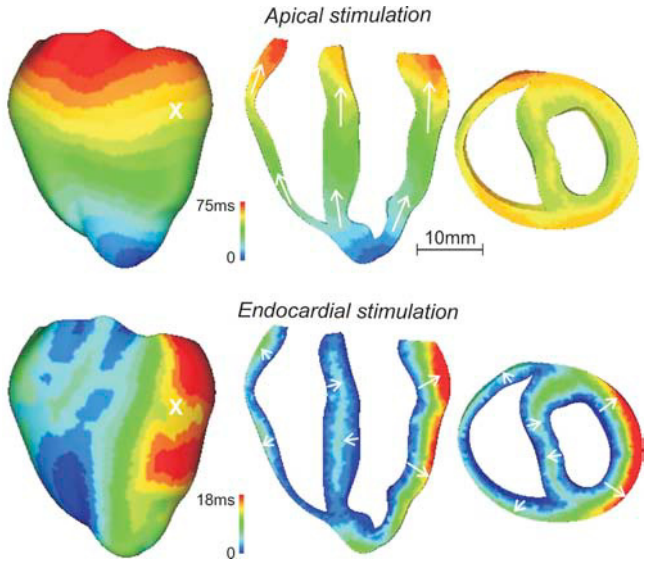

FIGURE 2 V_m activation maps after apical (*top*) and endocardial (*bottom*) stimulation. Arrows in transmural views indicate the direction of wavefront propagation. Crosses mark the epicardial node from which the action potentials in Fig. 3 were recorded. Locations of the slices through the ventricles are apex-base (*left*) and anterior-posterior (*right*) as shown in Fig. 1.

highlighted in Fig. 3 *B*. Firstly, the upstroke duration averaged over the epicardial nodes is larger for V_{opt} than V_m: it is 6.16 ms vs. 1.59 ms after apical stimulation, and 4.87 ms vs. 0.97 ms after endocardial stimulation, yielding τ_{opt} values of 3.86 and 5.01 for the respective protocols. Secondly, the morphology of the optical action potential upstroke changes slightly with the change in the direction of wavefront propagation with respect to the epicardium. For the traces shown in Fig. 3, the normalized value of V_{opt} at which the maximum upstroke velocity occurs is 0.58 after apical stimulation, and 0.55 after endocardial stimulation. In comparison, the normalized V_m value at which the maximum upstroke velocity occurs is 0.65 and 0.58 for the respective protocols. In both cases, the V_{opt} value of maximum upstroke velocity underestimates the corresponding V_m value; note that apical simulation results in marginally higher values for both V_{opt} and V_m signals.

Fig. 3 *C* depicts the epicardial distribution of V_m (*left*) and V_{opt} (*right*) 50 ms after apical stimulation (*top*) and 6 ms after endocardial stimulation (*bottom*). The prolongation of the optical action potential upstroke shown in Fig. 3, *A* and *B*, results in an increase in the optical wavefront width; the optical wavefront is 3.86 and 4.82 times wider for apical and endocardial stimulation, respectively.

In an optical mapping experiment, the amount of photon reflection and scattering close to the surface depends on the medium surrounding the heart, and specifically on the refractive index mismatch at the tissue-medium boundary. Implementation of the partial current boundary condition in our model allows us to quantify the changes in the ratio of the V_{opt} to V_m upstroke, τ_{opt}, with variation in refractive index mismatch R_{eff}. These results are shown in Fig. 4. Increasing R_{eff} from 0 to 0.95 results in an increase in τ_{opt} of 74% (from 3.64 to 6.33) for apical stimulation (*solid line*, *circles*) and 39% (from 4.83 to 6.72) for endocardial stimulation (*dashed line*, *squares*). The two most commonly used media to surround the heart in optical mapping experiments are glass and air, with relative refractive indices of 1.4 and 1.0, corresponding to values of $R_{eff} \approx 0$ and $R_{eff} \approx 0.5$, respectively. As demonstrated by Fig. 4, accounting for photon reflection at the surface through the use of the partial current boundary condition shows that using air instead of glass in an optical mapping experiment results in an increase in τ_{opt} (which is a measure of signal blurring) of ~6 and 4% for apical and endocardial stimulation, respectively.

It should be noted that in certain experimental scenarios, the heart is submerged in a bathing solution of perfusate, having a refractive index similar to that of water, i.e., $n = 1.3$. From the formulation for R_{eff} specified in Haskell et al. (10) we get $R_{eff} = 0.11$ for a tissue-perfusate interface, with corresponding τ_{opt} values seen in Fig. 4 very close to those of the tissue-glass interfaces for both protocols.

The two horizontal lines in Fig. 4, one for apical (*solid line*) and one for endocardial (*dashed line*) stimulation, correspond to values of τ_{opt} calculated using the zero boundary

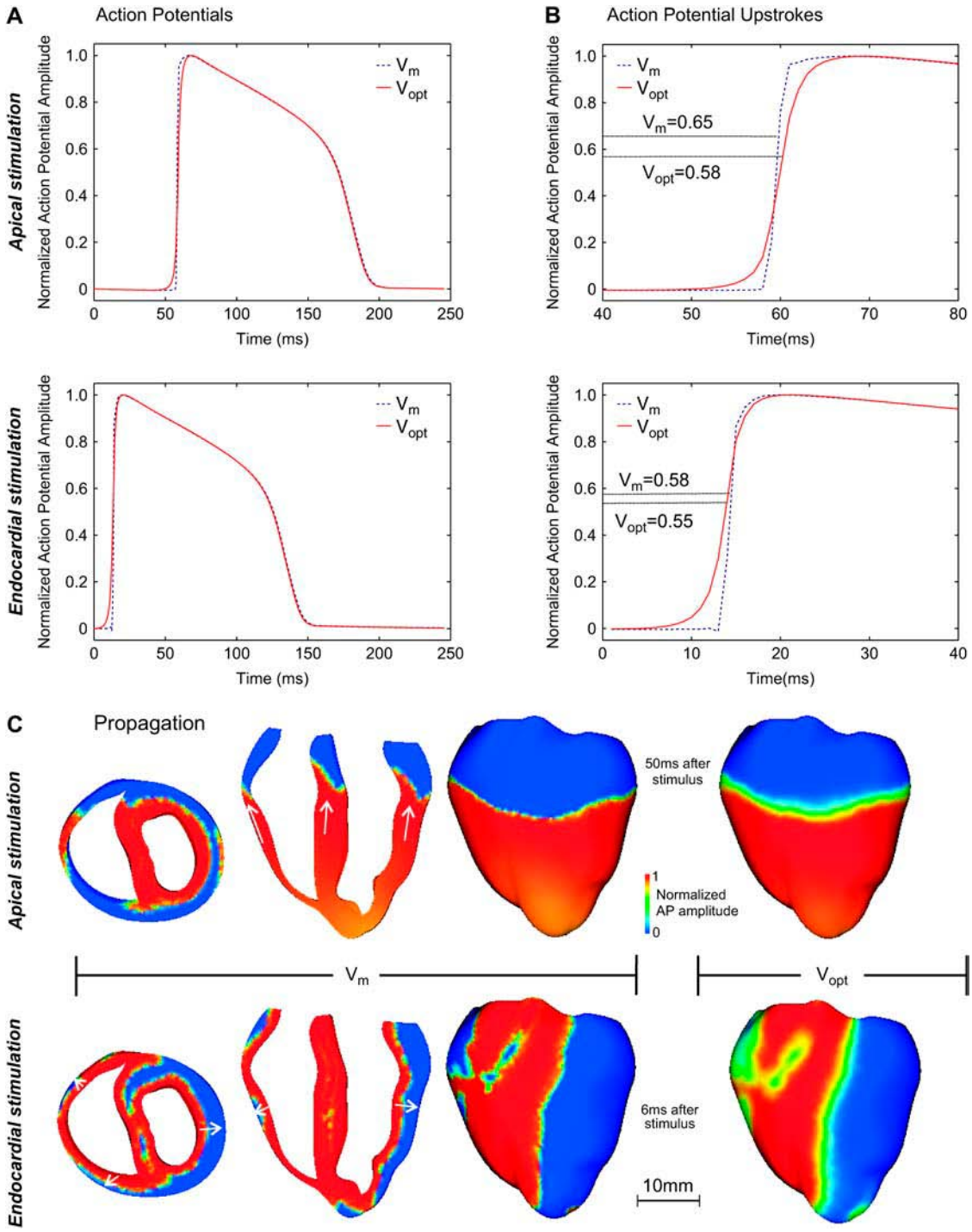

FIGURE 3 Epicardial transmembrane electrical activity (V_m) and fluorescent optical signal (V_{opt}) after apical (*top*) and endocardial (*bottom*) stimulus. (*A*) V_m and V_{opt} action potentials taken from epicardial node marked in Fig. 2, with the upstroke region highlighted in *B*. (*C*) Surface distribution of V_m (*left*) and V_{opt} (*right*) 50 ms after apical stimulation (*top*) and 6 ms after endocardial stimulation (*bottom*), including transmural views. Locations of the slices through the ventricles for the V_m images are apex-base (*right*) and anterior-posterior (*left*) as shown in Fig. 1.

condition on fluorescent emission employed in previous publications (5,7,12) instead of the more realistic partial current boundary condition used here. Solutions obtained using the zero boundary condition are independent of the surrounding medium. Our simulations show that using the zero boundary condition yields τ_{opt} of 3.53 and 4.74 for apical and endocardial stimulation, respectively. For an air-tissue interface, using the zero boundary condition therefore results

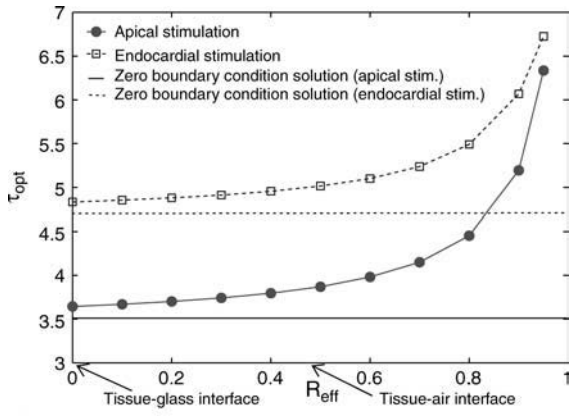

FIGURE 4 Variation of τ_{opt} with R_{eff} for apical (*solid line*, *circles*) and endocardial (*dashed line*, *squares*) stimulation protocols for the partial current boundary condition. Zero boundary condition solutions are also shown for the corresponding cases (*solid line* for apical, *dashed line* for endocardial stimulation).

in a reduction in the predicted blurring of the optical signal of ~9% for apical and 6% for endocardial stimulation, as compared to the case when the partial current boundary condition is used.

Photon scattering, and thus blurring in the optical signal, also depends on the characteristics of the experimental setup such as illumination and emission wavelengths, animal species, and individual characteristics of the tissue sample itself. These properties affect the light diffusivity and absorptivity parameters in our model, D and μ_a. Experimental values of these parameters vary in a large range, $0.05\ \text{mm} \le D \le 1.0\ \text{mm}$, $0.05\ \text{mm}^{-1} \le \mu_a \le 1.5\ \text{mm}^{-1}$ (4,11). We quantified the effect of varying D and μ_a within these ranges on τ_{opt}, separately during illumination and emission. This was done by varying the effective penetration depth δ_{eff}, defined as $\delta_{eff} = (D/\mu_a)^{1/2}$ (17). The expression for δ_{eff} is derived from the analytic solution to the photon diffusion equation, with a point source over a geometrically regular domain. For illumination, δ_{eff} is the photon penetration depth in the tissue. During emission, δ_{eff} represents the ease with which fluorescent photons can escape from the sample. For both stimulation protocols, δ_{eff} was fixed during the illumination process, while it was varied during the emission process, and vice-versa. Fig. 5 shows changes in τ_{opt} as the effective penetration depth δ_{eff} is varied independently during illumination (*dashed line*, *squares*) and emission (*solid line*, *circles*), for both apical (Fig. 5 *A*) and endocardial (Fig. 5 *B*) stimulation.

Fig. 5 demonstrates that for both illumination and emission, increasing δ_{eff} results in an increase in τ_{opt}. For both stimulation protocols, the greatest variation in τ_{opt} occurs for small values of δ_{eff} ($\le$1.5 mm), while a plateau is reached for large values of δ_{eff} ($\ge$2.5 mm). In addition, the emission process is more sensitive to changes in optical coefficients than the illumination process; this is more pronounced for

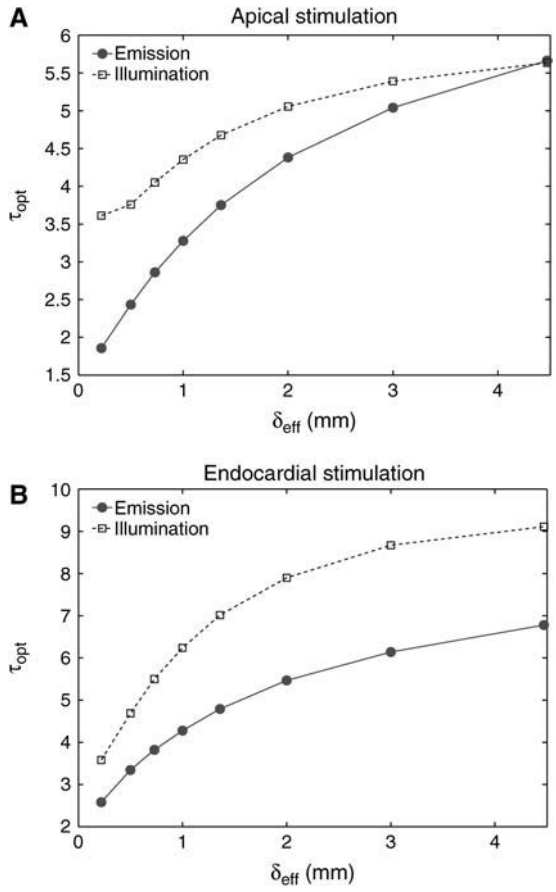

FIGURE 5 Variation of τ_{opt} as the scattering properties of the tissue are varied. The penetration depth δ_{eff} (defined as $(D/\mu_a)^{1/2}$) during illumination and emission is varied individually for both apical and endocardial stimulation protocols. Panel *A* plots τ_{opt} vs. δ_{eff} during illumination and emission for apical stimulation; *B* shows the same for endocardial stimulation.

apical stimulation than for endocardial. As δ_{eff} varies between 0.22 mm and 4.47 mm, τ_{opt} changes by 205 and 163% during emission, for apical and endocardial stimulation, respectively, compared to 56 and 154% during illumination.

DISCUSSION

In this study, a model of photon scattering for illumination and emission is used for the first time in combination with an anatomically based bi-domain model of the rabbit ventricles to simulate fluorescent signals over the entire epicardium. The model incorporates the partial current boundary condition enabling realistic representation of the interface between epicardial tissue and surrounding medium for different types of experimental setups. Using this model, we quantified the changes in fluorescent signal distortion for varying light absorption and diffusivity in cardiac tissue, and for changes in refractive index mismatch between cardiac tissue and the surrounding medium. These results aim to provide better interpretation of optical mapping experiments, and are made possible through the use of realistic geometrical information.

Consistent with previous experimental and theoretical studies (5,6,18), our results show that fluorescent photon scattering leads to optical signal distortion, and specifically, to prolongation of action potential upstroke and thus to an increase in the width of the propagating wavefront. In our simulations for an air-tissue interface, optical action potential upstroke durations were found to be in the range of ~3–9 times longer than the V_m action potential upstroke durations. This range of values is in close agreement with experimental results by Girouard et al. (18), who compared optical upstrokes to those recorded with microelectrodes. In addition, values of τ_{opt} for apical stimulation (3.86) and for endocardial stimulation (5.01) match closely to the value of $\tau_{opt} \approx 5$ found from a previous simulation study of photon scattering in sheep myocardium by Hyatt et al. (5). The values of ω_{opt}, a measure of the increase in the width of the propagating activation wavefront, of 3.86 for apical and 4.82 for endocardial stimulation, also agreed well with the value of $\omega_{opt} \approx 3$ found in the same study (5). Further validation of our model came from specific consideration of photon scattering during illumination over our irregular geometry model, which yielded a fitted penetration depth of $\delta = 0.57$ mm. This value is in accordance with the value of the effective penetration depth for rabbit myocardium, 0.59 mm, calculated as $\delta_{eff} = (D/\mu_a)^{1/2}$ with experimentally measured values of D and μ_a (4). The fitted value of δ differs slightly from the experimentally measured penetration depths found in other species such as sheep, 0.8 mm (3), and guinea-pig, 0.29 mm (18), due to species-dependent differences in the values of D and μ_a.

The degree of photon scattering which causes the distortion in the optical signal, depends critically upon the optical parameters D and μ_a, and thus on the effective penetration depth at both illumination and emission wavelengths. The depth of penetration of the illuminating light, and the ease with which emitted fluorescent photons exit the deeply excited layers, govern the total degree of distortion in optical signals. By varying the optical parameters between limits encountered experimentally for different samples, it was possible to assess the effects of different values of D and μ_a, at both the illumination and emission wavelengths, on the value of τ_{opt}, which relates directly to the degree of photon scattering in the tissue. A significant change in τ_{opt} was found over the range of penetration depths, from a minimum of 2.58 to a maximum of 9.11, demonstrating the sensitivity of the model to the input parameters. In addition to large variations between species (11), the estimated values of the optical coefficients at different wavelengths vary also for the same type of tissue (4). Therefore, knowledge of how blurring depends on the effective penetration depths (related directly to D and μ_a) during illumination and emission is of paramount importance, and should be considered when using these experimentally obtained optical parameters in scattering models such as the one presented in this study. Furthermore, such dependence of distortion upon optical parameters is important when selecting dyes that have different excitation/emission wavelengths and correspondingly different penetration depths.

The depth from which optical signals originate is an important factor to consider when presented with episodes of heterogeneous transmembrane potential distribution within the myocardium, such as those resulting from defibrillation shocks. In such cases, there is a great variation in V_m throughout the three-dimensional volume beneath the recording site from which the scattered photons emanate. These scattered photons transduce the differences in transmembrane potential within this volume into the recorded signal via fluorescent scattering, leading to a large degree of blurring in the optical signal. Thus, when there is a large change in V_m in a transmural direction beneath the recording site, the depth from which the scattered photons originate will determine the degree to which the fluorescent signal is distorted.

Altering the penetration depth during illumination allows explicit control over the depth of tissue that is excited by the illuminating photons. Fig. 5 shows that even for a very small value of the illumination penetration depth such as 0.22 mm, τ_{opt} is still relatively large: it is 3.61 for apical stimulation and 3.58 for endocardial. For such values of δ_{eff} the illuminating photons are only able to excite the outermost layers of tissue, therefore it is fluorescent photon scattering in the plane of the epicardium, not from depth, that mainly contributes to the distortion of the optical signal. This effect could help explain the significant prolongation of the optical action potential upstroke observed in thin cell-culture recordings, where scattering from the depth is an unlikely cause of signal distortion.

The three-dimensional nature of the fluorescent photon scattering is also underscored by the similarities between the two stimulation protocols in the dependence of τ_{opt} on the input optical parameters D, μ_a, and R_{eff}. The two protocols result in very different directions of wavefront propagation with respect to the epicardium (Fig. 2) and thus there are large differences in the transmural distribution of V_m beneath the recording site (Fig. 3 *C*): propagation parallel to the epicardium results in a small transmural change in V_m beneath an epicardial recording site, whereas propagation toward the epicardium results in a large change in V_m between endo- and epicardium. Therefore, scattering in the epicardial plane is the prevalent direction of scattering for apical stimulation, while scattering from depth predominates for endocardial stimulation. Nonetheless, these two different directions of scattering yield similar values of τ_{opt} for the default parameter set. In addition, we also find a very similar overall change in τ_{opt} in response to the parameter changes shown in Figs. 4 and 5. Therefore, the results of our study underscore the truly three-dimensional nature of the fluorescent photon scattering and place a high emphasis on the use of an accurate ventricular geometry over which the optical signals are synthesized. In this respect, our study represents a significant improvement over earlier works, which used simple

transmural depth-averaging techniques to predict the characteristics of optical signals (6,19); these only considered scattering in one dimension directly beneath the recording site. It should be noted at this point that the effects of averaging over a pixel of finite area upon detection have not been accounted for, which would add to the lateral distortion seen in the epicardium plane.

Studies by Hyatt et al. (5,7) showed that, through the morphology of the optical action potential upstroke, fluorescent photon scattering can transduce important information regarding transmural wavefront propagation. The study by Hyatt et al. (7) investigated, using a simplified three-dimensional slab computer model, the effect of changing the orientation of a planar wavefront on the optical action potential upstroke morphology. For propagation perpendicular to the recording surface, the authors found the level of normalized depolarization at which maximum upstroke velocity is reached in the optical signal to be 0.48, compared to 0.85 for propagation toward the recording surface. Our simulations did not find such a large change in upstroke characteristics allowing the change in wavefront direction; the corresponding values for apical and endocardial stimulation found here were 0.58 and 0.55, respectively. The reason for the discrepancy between the findings of our study and these in Hyatt et al. (7) is that in our model, where geometry and fiber orientation are anatomically based, wavefronts do not propagate in directions exactly parallel or perpendicular to the epicardium, although the stimulation protocols were specifically chosen to elicit wavefronts which were as close to parallel/perpendicular to the epicardium as possible. Our results therefore demonstrate that information obtained from optical upstroke morphology is not a reliable indicator of near-surface transmural propagation direction when whole-heart models with realistic geometry and fiber orientation are used.

The refractive index mismatch between the heart and the surrounding medium in an optical mapping experiment determines the degree of fluorescent photon reflection at the boundary. Photons which are reflected back into the tissue at the epicardium will affect scattering close to the surface, and hence the degree of distortion in the optical signal. The implementation of the partial current boundary condition accounts for this additional reflection through the parameter R_{eff}, allowing different experimental setups to be simulated. Increasing the refractive index mismatch (and hence R_{eff}) in our simulations results in an increase in τ_{opt} due to increased reflection and fluorescent photon scattering close to the surface. As a result, experimental setups that use air-tissue interfaces ($R_{\text{eff}} \approx 0.5$) were found to have 6 and 4% larger blurring of the optical signal for apical and endocardial stimulation, respectively, compared to glass-tissue interfaces ($R_{\text{eff}} \approx 0$). Previous theoretical studies have used the zero boundary condition to solve the photon diffusion equation for fluorescent emission (5,7,12). The zero boundary condition fails to account for any form of reflection due to the refractive index mismatch at the tissue surface, in addition to the inability to represent different experimental setups. As shown here, the use of the zero boundary condition underestimates the blurring in the fluorescent signal by up to 9% for glass or air interfaces with the myocardium.

In conclusion, this study provides insight into the mechanisms and underlying physical processes responsible for the blurring and distortion effects seen in experimentally recorded optical signals. The use of accurate ventricular geometry and fiber orientation in the model is essential in representing the complex pattern of propagation in the heart and its effect on the optically recorded signal. Furthermore, the partial current boundary condition provides an accurate representation of the experimental setup; it is highly flexible and can be adapted to model various experimental scenarios. To allow direct comparison to experimental data, accurate knowledge of the input parameters in the model that are specific to each experimental setup is imperative. This is particularly important when using the model to examine the modulation of fluorescent recordings during episodes of highly irregular transmembrane potential distribution, such as after defibrillation shocks. The use of the realistic modeling tool presented here provides an opportunity to accurately simulate such distortion effects in the optical signal.

The authors are pleased to acknowledge the support of the United Kingdom Engineering and Physical Sciences Research Council through a Life Sciences Interface Doctoral Training Centre studentship (No. GR/S58119/01 to M.J.B.) and the Integrative Biology E-Science pilot project (No. GR/S72023/01 to D.J.G.), in addition to the National Institutes of Health (grants No. HL063195, No. HL074283, and No. HL067322 to N.T.) and the Whitaker Foundation and the Jeffress Memorial Trust (to J.E.).

REFERENCES

1. Loew, L. M. 2001. Optical mapping of cardiac excitation and arrhythmias. *In* Mechanisms and Principles of Voltage-Sensitive Fluorescence. Futura Publishing, Armonk, NY. 33–46.
2. Efimov, I., V. Nikolski, and G. Salama. 2004. Optical imaging of the heart (review). *Circ. Res.* 94:21–33.
3. Baxter, W., S. Mironov, A. Zaitsev, J. Jalife, and A. Pertsoz. 2001. Visualizing excitation waves inside cardiac muscle using transillumination. *Biophys. J.* 80:516–530.
4. Ding, L., R. Splinter, and S. Knisley. 2001. Quantifying spatial localization of optical mapping using Monte Carlo simulations. *IEEE Trans. Biomed. Eng.* 48:1098–1107.
5. Hyatt, C., S. Mironov, M. Wellner, O. Berenfeld, A. Popp, D. Weitz, J. Jalife, and A. Pertsov. 2003. Synthesis of voltage-sensitive fluorescence signals from three-dimensional myocardial activation patterns. *Biophys. J.* 85:2673–2683.
6. Bray, M., and J. Wikswo. 2003. Examination of optical depth effects on fluorescence imaging of cardiac propagation. *Biophys. J.* 85:4134–4145.
7. Hyatt, C., S. Mironov, F. Vetter, C. Zemlin, and A. Pertsov. 2005. Optical action potential upstroke morphology reveals near-surface transmural propagation direction. *Circ. Res.* 97:277.
8. Trayanova, N., J. Eason, and F. Aguel. 2002. Computer simulations of cardiac defibrillation: a look inside the heart. *Comput. Visual Sci.* 4: 259–270.
9. Ashihara, T., and N. Trayanova. 2004. Asymmetry in membrane responses to electric shocks: insights from bi-domain simulations. *Biophys. J.* 87:2271–2282.

10. Haskell, R., L. Svaasand, T. Tsay, T. Feng, M. McAdams, and B. Tromberg. 1994. Boundary conditions for the diffusion equation in radiative transfer. *Opt. Soc. Am.* 11:2727–2741.

11. Cheong, W., S. Prahl, and A. Welch. 1990. A review of the optical properties of biological tissues. *IEEE J. Quant. Electron.* 26:2166–2185.

12. Bernus, O., M. Wellner, S. Mironov, and A. Pertsov. 2005. Simulation of voltage-sensitive optical signals in three-dimensional slabs of cardiac tissue: application of transmural and coaxial imaging methods. *Phys. Med. Biol.* 50:215–229.

13. Kay, M., P. Amison, and J. Rogers. 2004. Three-dimensional surface reconstruction and panoramic optical mapping of large hearts. *IEEE Trans. Biomed. Eng.* 51:1219–1229.

14. Lin, S. F., and J. P. Wikswo, Jr. 1999. Panoramic optical imaging of electrical propagation in isolated heart. *J. Biomed. Opt.* 4:200–207.

15. Chattipakorn, N., I. Banville, R. Gray, and R. Ideker. 2001. Mechanism of ventricular defibrillation for near-defibrillation threshold shocks: a whole-heart optical mapping study in swine. *Circulation.* 104:1313–1319.

16. Efimov, I., V. Sidorov, Y. Cheng, and B. Wollenzier. 1999. Evidence of three-dimensional scroll waves with ribbon-shaped filaments as a mechanism of ventricular tachycardia in isolated rabbit heart. *J. Cardiovasc. Electrophysiol.* 10:1451–1462.

17. Jacques, S. 1998. Light distributions from point, line and plane sources for photochemical reactions and fluorescence in turbid biological tissues. *Photochem. Photobiol.* 67:23–32.

18. Girouard, S., K. Laurita, and D. Rosenbaum. 1996. Unique properties of cardiac action potentials with voltage-sensitive dyes. *J. Cardiovasc. Electrophysiol.* 7:1024–1038.

19. Janks, D., and B. Roth. 2002. Averaging over depth during optical mapping of unipolar simulation. *IEEE Trans. Biomed. Eng.* 49:1051–1054.